



Enhanced Voltage Control of VSC-HVDC Connected Offshore Wind Farms Based on Model Predictive Control

Guo, Yifei; Gao, Houlei; Wu, Qiuwei; Zhao, Haoran; Østergaard, Jacob; Shahidehpour, Mohammad

Published in:
IEEE Transactions on Sustainable Energy

Link to article, DOI:
[10.1109/TSTE.2017.2743005](https://doi.org/10.1109/TSTE.2017.2743005)

Publication date:
2018

Document Version
Peer reviewed version

[Link back to DTU Orbit](#)

Citation (APA):
Guo, Y., Gao, H., Wu, Q., Zhao, H., Østergaard, J., & Shahidehpour, M. (2018). Enhanced Voltage Control of VSC-HVDC Connected Offshore Wind Farms Based on Model Predictive Control. *IEEE Transactions on Sustainable Energy*, 9(1). <https://doi.org/10.1109/TSTE.2017.2743005>

General rights

Copyright and moral rights for the publications made accessible in the public portal are retained by the authors and/or other copyright owners and it is a condition of accessing publications that users recognise and abide by the legal requirements associated with these rights.

- Users may download and print one copy of any publication from the public portal for the purpose of private study or research.
- You may not further distribute the material or use it for any profit-making activity or commercial gain
- You may freely distribute the URL identifying the publication in the public portal

If you believe that this document breaches copyright please contact us providing details, and we will remove access to the work immediately and investigate your claim.

Enhanced Voltage Control of VSC-HVDC Connected Offshore Wind Farms Based on Model Predictive Control

Yifei Guo, Houlei Gao, *Member, IEEE*, Qiuwei Wu, *Senior Member, IEEE*, Haoran Zhao, Jacob Østergaard, *Senior Member, IEEE*, and Mohammad Shahidepour, *Fellow, IEEE*

Abstract—This paper proposes an enhanced voltage control strategy (EVCS) based on model predictive control (MPC) for voltage source converter based high voltage direct current (VSC-HVDC) connected offshore wind farms (OWFs). In the proposed MPC based EVCS, all wind turbine generators (WTGs) as well as the wind farm side VSC are optimally coordinated to keep voltages within the feasible range and reduce system power losses. Considering the high R/X ratio of the OWF collector system, the effects of active power outputs of WTGs on voltage control are also taken into consideration. The predictive model of VSC with a typical cascaded control structure is derived in details. The sensitivity coefficients are calculated by an analytical method to improve the computational efficiency. A VSC-HVDC connected OWF with 64 WTGs was used to validate the proposed voltage control strategy.

Index Terms—model predictive control (MPC), offshore wind farms (OWFs), power loss, voltage control, VSC-HVDC.

I. INTRODUCTION

WIND power has been rapidly developing during last few decades due to the renewable-energy targets set by the governments over the world. A considerable number of large scale wind farms are planned distant from the onshore grid [1]. Compared with conventional submarine high voltage AC transmission, the voltage source converter-based high voltage direct current (VSC-HVDC) transmission system is considered as a suitable way to transport the power from distant offshore wind farms (OWFs) due to various techno-economic advantages such as independent active and reactive power control, frequency decoupling between OWFs and onshore grids, feasibility of multi-terminal dc grids and inherent black start capability [2]-[3].

This work was supported by the National Key Research and Development Program of China under Grant 2016YFB0900603.

Y. Guo and H. Gao are with Key Laboratory of Power System Intelligent Dispatch and Control of Ministry of Education, Shandong University, Jinan 250061, China (e-mail: yfguo_sdu@163.com; houlei@163.com).

Q. Wu is with the Center for Electric and Energy, Department of Electrical Engineering, Technical University of Denmark (DTU), Kgs. Lyngby 2800, Denmark, and School of Electrical Engineering, Shandong University, Jinan 250061, China (e-mail: qw@elektro.dtu.dk).

H. Zhao and J. Østergaard are with Center for Electric and Energy, Department of Electrical Engineering, Technical University of Denmark (DTU), Kgs. Lyngby 2800, Denmark (e-mail: hzhao@elektro.dtu.dk; joe@elektro.dtu.dk).

M. Shahidepour is with the Department of Electrical and Computer Engineering, Illinois Institute of Technology (IIT), Chicago, IL 60616, USA (e-mail: ms@iit.edu).

The increased penetration of wind power in power systems has introduced various challenges towards system operation [4]. To counter the challenges, modern wind farms are required to meet the grid code requirements [5]-[7] set by transmission system operators (TSOs). In conventional AC connected wind farms, the active power and reactive power (Var) control are decoupled [8]. Generally, the active power of wind farms is required to track the reference set by system operators. The total active power is dispatched to individual wind turbine generators (WTGs) by the wind farm active power controller. Several dispatch strategies such as proportional distribution (PD) control, proportional-integral (PI) control and fuzzy control, have been discussed in [9]. Among these, the PD strategy is widely adopted in modern wind farms due to its simple implementation, which also takes into account the available power and Var capability of WTGs [8]-[11]. Reactive power control is related to the voltage regulation of wind farms. Several control modes including voltage, power factor and reactive power at the point of connection (POC) have been specified in many grid codes [12]. Voltage control mode often shows superior performance for transmission systems [13]. In [11], [14], the set-point of reactive power was calculated based on the voltage at the POC and then dispatched to each WTG based on the PD strategy which is similar to the active power dispatch. Centralized and decentralized voltage control schemes were discussed in [15], which are distinguished by the outer control loop of WTGs. The decentralized control scheme performs better considering the negligible delay between wind farm controller and WTGs. In [16], a hierarchical voltage controller was designed and implemented in a wind power base of northern China.

For VSC-HVDC connected OWFs, a considerable number of studies have been done for the fault ride through (FRT) / low voltage ride through (LVRT) control strategies due to the lower short circuit power contribution from power electronic interfaced WTGs and VSCs [17]-[19].

The control strategies based on optimal power flow (OPF) were proposed in [20]-[23]. In [20], the voltage reference of the pilot bus was determined by the offline optimal power flow calculation and the total reactive power reference was obtained using a PI controller and then dispatched to each WTG. In [21]-[23], the objectives of the OPF were the power loss of the OWF collector system, grid side converter (GSC) of WTGs and HVDC converters. Since the VSC-HVDC transmission system decouples the OWFs from the onshore

AC grid, the main control aim for OWFs is to maintain the terminal voltage of each WTG within the feasible range [16], which was not considered in these OPF-based strategies. Besides, generally, the voltage of POC controlled by wind farm side VSC (WVSC) is set at the nominal value [24], which may neglect the fast voltage adjustment capability of VSC.

In recent years, Model Predictive Control (MPC), also called receding horizon control, has been extensively applied in the wind power generation system both at the wind turbine level [25]-[28] and wind farm level [13], [29]-[31]. In [25], a model-based predictive controller for power control of doubly fed induction generator (DFIG)-based WTG was proposed using a linearized state-space model. In [26], a new wind power conversion system configuration was explored and a two-step model predictive control strategy was proposed, which optimizes the maximum power point tracking (MPPT), dc-link capacitor voltages balancing, regulation of net dc-bus voltage, etc. In [27], a nonlinear model predictive controller was derived for power control of DFIG, taking into account the unbalanced grid conditions. Similarly, in [28], a direct power control strategies under unbalanced grid voltage conditions was proposed based on MPC. A distributed MPC scheme of a wind farm for optimal active power control using the fast gradient method was proposed in [29]-[30]. The objectives of the wind farm controller are power reference tracking from the system operator and WTG mechanical load minimization. In [13], a MPC-based coordinated wind farm voltage controller was designed to optimally coordinate different fast and slow voltage regulation devices. In [31], a combined power control strategy was proposed to optimize the voltage profile inside the wind farm as well as the fatigue loads of WTGs.

The MPC can be effectively applied in the wind power generation system due to the following advantages:

- The control objective and operating constraints can be explicitly represented in the optimization problem [32];
- It can take into account the dynamic response of the system, consequently, the obtained optimal control input is more effective than that without prediction;
- It is applicable both at the turbine level and farm level and can be designed with different time scales.
- It is suitable to optimally coordinate various Var devices in a wind farm with different time constants [13], [31].

The main contribution of this paper is a MPC based enhanced voltage control strategy (MPC-EVCS) design for VSC-HVDC connected OWFs. The WVSC and WTGs are optimally coordinated in this strategy. The impacts of active power output of WTGs on voltage variation are also taken into consideration to improve the voltage control performance. The predictive VSC model with the common cascaded control structure is developed. The sensitivity coefficients with respect to power injections and slack bus voltage are derived based on an analytical method. Compared to the existing control strategies, the proposed strategy can regulate voltages while also taking into account economic operation of the OWFs. And the fast and flexible voltage regulation capability of the VSC can be fully used. Besides, the active and reactive

power outputs of WTGs are optimally coordinated to achieve better control performance.

The rest of this paper is organized as follows. In Section II, the concept of the proposed MPC-EVCS is presented. In Section III, the sensitivity calculation method is introduced. In Section IV, the predictive models of VSC and WTGs are developed. The mathematical formulation of the MPC-EVCS is presented in Section V. Section VI presents the case studies followed by conclusions.

II. MPC BASED ENHANCED VOLTAGE CONTROL STRATEGY FOR VSC-HVDC CONNECTED OWFS

A. Configuration of the VSC-HVDC Connected OWFs

Fig. 1 shows the typical configuration of a VSC-HVDC connected OWF, which is connected to the onshore external 400 kV AC grid through a ± 150 kV VSC-HVDC system with nominal power rating of 400 MW. The OWF is comprised of two parts. Each part is equipped with a collector substation, and the substations are connected to a common VSC station through 150 kV submarine cables. The WTGs are connected by eight medium voltage (MV) 33 kV collector cables. There are eight full-scale-converter 6.25 MW WTGs at each feeder, referred to as a string. The WTGs are placed with a distance of 1.5 km.

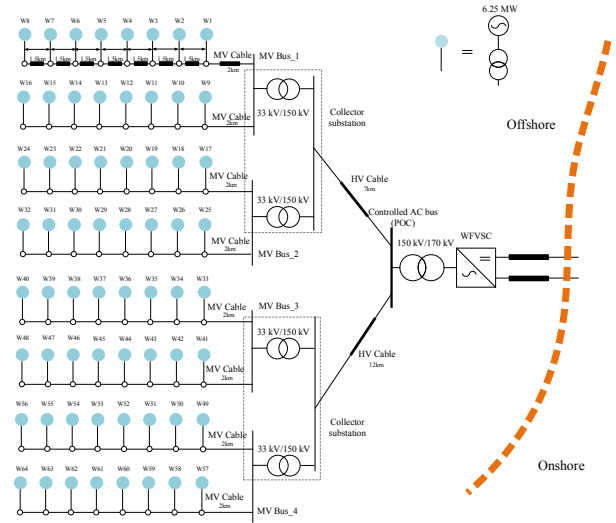


Fig. 1. Configuration of a VSC-HVDC connected OWF.

B. Concept of the MPC-EVCS

The structure of the MPC controller is illustrated in Fig. 2. In the proposed MPC controller, there are two control modes designed for different operation conditions: 1) normal mode, and 2) corrective mode. In the first control mode, all bus voltages are within the feasible range. The control objective is to minimize voltage deviations of the key buses, reduce system power losses and optimize the active power distribution of WTGs. In the corrective mode, the control objective is to correct the bus voltage which violates the limits. A dynamic weighting coefficient allocation method according to the degree of voltage deviation is used to regulate the voltage more effectively. The details of the proposed MPC-

EVCS are presented in Section V. To be noticed, the control period of the proposed EVCS is in seconds. Considering the real-life implementation, the coordination between the EVCS and existing FRT control scheme [17]-[20] of a wind farm should be in place. The FRT control should have the highest priority. Once one unit triggers the FRT control strategy, the EVCS will be locked. The control mode will switch to the FRT control mode. A voltage dead-band can be designed to coordinate these two control strategies.

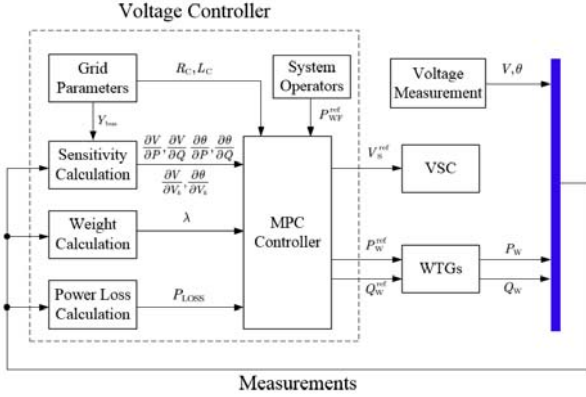


Fig. 2. Structure of the OWF voltage control.

III. SENSITIVITY COEFFICIENT CALCULATION

The calculation of voltage sensitivity, active power losses sensitivity and Var limit sensitivity of WTGs is presented in this section.

A. Voltage Sensitivity

In the typical optimal control problems, the updated Jacobian matrix is commonly used to derive the voltage sensitivity coefficients. From the computational point of view, the main disadvantage of this method is that the Jacobian matrix should be rebuilt and inverted for every change in operation conditions of the network, which involves non-trivial computation constraints for the implementation in real-time control problems. Moreover, this method cannot be used to calculate the sensitivity coefficients with respect to slack bus voltage. Thus, an efficient analytical sensitivity calculation method, which was initially used in radial distribution network, is used in this paper to improve the computation efficiency [33].

Considering a network comprised of N buses (N_S slack buses and N_{PQ} buses with PQ injections). \mathcal{S} and \mathcal{N} denote the sets of slack buses and the buses with PQ injections, respectively, i.e., $\mathcal{S} \cup \mathcal{N} = \{1, 2, \dots, N\}$ with $\mathcal{S} \cap \mathcal{N} = \emptyset$. Define $\bar{V}_i \triangleq V_i e^{j\theta_i}$ for all buses and $\bar{S}_i = P_i + jQ_i$ for $i \in \mathcal{N}$. The link between bus voltages and power injections is

$$\underline{S}_i = \underline{V}_i \sum_{j \in \mathcal{S} \cup \mathcal{N}} \bar{Y}_{bus,ij} \bar{V}_j \quad (1)$$

where \underline{V}_i and \underline{S}_i denote the conjugates of \bar{V}_i and \bar{S}_i , respectively; $Y_{bus} = [\bar{Y}_{bus,ij}]_{N \times N}$ denotes the admittance matrix.

a. Sensitivity coefficients with respect to power injections

To derive the voltage magnitude and phase angle sensitivity coefficients with respect to power injections, the partial derivatives of \underline{S}_i ($i \in \mathcal{N}$) with respect to active power P_l and reactive power Q_l of a bus $l \in \mathcal{N}$ have to be calculated, which satisfy the following equations:

$$\begin{aligned} \frac{\partial \underline{S}_i}{\partial P_l} &= \frac{\partial \{P - jQ\}}{\partial P_l} = \frac{\partial V_i}{\partial P_l} \sum_{j \in \mathcal{S} \cup \mathcal{N}} \bar{Y}_{bus,ij} \bar{V}_j \\ &\quad + \bar{V}_i \sum_{j \in \mathcal{N}} \bar{Y}_{bus,ij} \frac{\partial \bar{V}_j}{\partial P_l} = \begin{cases} 1, & \text{for } i = l. \\ 0, & \text{for } i \neq l. \end{cases} \end{aligned} \quad (2)$$

$$\begin{aligned} \frac{\partial \underline{S}_i}{\partial Q_l} &= \frac{\partial \{P - jQ\}}{\partial Q_l} = \frac{\partial V_i}{\partial Q_l} \sum_{j \in \mathcal{S} \cup \mathcal{N}} \bar{Y}_{bus,ij} \bar{V}_j \\ &\quad + \bar{V}_i \sum_{j \in \mathcal{N}} \bar{Y}_{bus,ij} \frac{\partial \bar{V}_j}{\partial Q_l} = \begin{cases} -j1, & \text{for } i = l. \\ 0, & \text{for } i \neq l. \end{cases} \end{aligned} \quad (3)$$

Equation (2) is linear with respect to $\partial \bar{V}_i / \partial P_l$ and $\partial V_i / \partial P_l$. Equation (3) is linear with respect to $\partial \bar{V}_i / \partial Q_l$ and $\partial V_i / \partial Q_l$. According to the theorem in [33], (2) and (3) have a unique solution for radial network.

Once $\partial \bar{V}_i / \partial P_l$, $\partial V_i / \partial P_l$, $\partial \bar{V}_i / \partial Q_l$ and $\partial V_i / \partial Q_l$ are obtained, the voltage magnitude and phase angle sensitivity can be computed by,

$$\frac{\partial V_i}{\partial P_l} = \frac{1}{V_i} \text{Re} \left(\underline{V}_i \frac{\partial \bar{V}_i}{\partial P_l} \right), \quad \frac{\partial \theta_i}{\partial P_l} = \frac{1}{V_i^2} \text{Im} \left(\underline{V}_i \frac{\partial \bar{V}_i}{\partial P_l} \right) \quad (4)$$

$$\frac{\partial V_i}{\partial Q_l} = \frac{1}{V_i} \text{Re} \left(\underline{V}_i \frac{\partial \bar{V}_i}{\partial Q_l} \right), \quad \frac{\partial \theta_i}{\partial Q_l} = \frac{1}{V_i^2} \text{Im} \left(\underline{V}_i \frac{\partial \bar{V}_i}{\partial Q_l} \right) \quad (5)$$

b. Sensitivity coefficients with respect to slack bus voltage

For a bus $i \in \mathcal{N}$, the partial derivatives with respect to voltage magnitude V_k of a slack bus $k \in \mathcal{S}$ are derived by,

$$-\bar{V}_i \bar{Y}_{bus,ik} e^{j\theta_k} = \underline{W}_{ik} \sum_{j \in \mathcal{S} \cup \mathcal{N}} \bar{Y}_{bus,ij} \bar{V}_j + \underline{V}_i \sum_{j \in \mathcal{N}} \bar{Y}_{bus,ij} \bar{W}_{jk} \quad (6)$$

where

$$\bar{W}_{ik} = \frac{\partial \bar{V}_i}{\partial V_k} = \left(\frac{1}{V_i} \frac{\partial V_i}{\partial V_k} + j \frac{\partial \theta_i}{\partial V_k} \right) \bar{V}_i.$$

Equation (6) is linear with respect to \bar{W}_{ik} and \underline{W}_{ik} , and also has a unique solution. By solving it, the sensitivity coefficients with respect to the slack bus voltage magnitude at bus k are calculated by,

$$\frac{\partial V_i}{\partial V_k} = V_i \text{Re} \left(\frac{\bar{W}_{ik}}{\bar{V}_i} \right), \quad \frac{\partial \theta_i}{\partial V_k} = \text{Im} \left(\frac{\bar{W}_{ik}}{\bar{V}_i} \right). \quad (7)$$

B. Active Power Losses Sensitivity

The power losses of the grid (cables and transformers) and power losses of the converters (GSCs of WTGs and WFVSC) are considered in the paper.

a. Power losses of grid

The partial derivatives of power losses with respect to voltage magnitude and phase angle can be calculated by,

$$\frac{\partial P_{\text{Grid}}^{\text{LOSS}}}{\partial V_i} = 2 \sum_{j=1}^N V_j G_{ji} \cos \theta_{ji}, \quad (8a)$$

$$\frac{\partial P_{\text{Grid}}^{\text{LOSS}}}{\partial \theta_i} = 2 \sum_{j=1}^N V_i V_j G_{ji} \sin \theta_{ji}. \quad (8b)$$

where G_{ij} is the real part of \bar{Y}_{ij} and $\theta_{ji} = \theta_j - \theta_i$.

Then, the sensitivity with respect to power output of WTGs and terminal voltage of WfVSC can be calculated by combing (4)-(8), which is as follows

$$\frac{\partial P_{\text{Grid}}^{\text{LOSS}}}{\partial y} = \frac{\partial P_{\text{Grid}}^{\text{LOSS}}}{\partial V} \cdot \frac{\partial V}{\partial y} + \frac{\partial P_{\text{Grid}}^{\text{LOSS}}}{\partial \theta} \cdot \frac{\partial \theta}{\partial y}, \quad (9)$$

where y represents the active/reactive power output of WTGs and terminal voltage of WfVSC (the slack bus voltage).

b. Power losses of converters

The GSC of each WTG and HVDC converters are two-level VSCs. The converter loss can be approximated by a quadratic function depending on the converter current I_C (in p.u.) [21],

$$P_{\text{Conv}}^{\text{LOSS}} = \left(a + b \left(\frac{I_{\text{Conv}}}{I_R} \right) + c \left(\frac{I_{\text{Conv}}}{I_R} \right)^2 \right) S_{\text{Conv}}, \quad (10)$$

$$I_{\text{Conv}} = \frac{\sqrt{P_{\text{Conv}}^2 + Q_{\text{Conv}}^2}}{V_{\text{Conv}}}, \quad (11)$$

where I_R is the rated converter current, S_{Conv} denotes the nominal capacity. P_{Conv} , Q_{Conv} , and V_{Conv} are the power injections and terminal voltage. a , b , and c are the converter loss parameters which are presented in Appendix B.

According to (11), the converter loss is related to the power injections and terminal voltage. Considering the terminal voltage is always around 1.0 p.u during normal operation, its impacts are neglected, and then the converter loss sensitivity can be calculated by,

$$\begin{aligned} \frac{\partial P_{\text{Conv}}^{\text{LOSS}}}{\partial P_{\text{Conv}}} &= \frac{\partial P_{\text{Conv}}^{\text{LOSS}}}{\partial I_{\text{Conv}}} \cdot \frac{\partial I_{\text{Conv}}}{\partial P_{\text{Conv}}} \\ &= \left(\frac{b}{I_R} + 2c \frac{I_{\text{Conv}}}{I_R} \right) S_{\text{Conv}} \cdot \frac{P_{\text{Conv}}}{V_{\text{Conv}} \sqrt{P_{\text{Conv}}^2 + Q_{\text{Conv}}^2}} \end{aligned} \quad (12)$$

$$\begin{aligned} \frac{\partial P_{\text{Conv}}^{\text{LOSS}}}{\partial Q_{\text{Conv}}} &= \frac{\partial P_{\text{Conv}}^{\text{LOSS}}}{\partial I_{\text{Conv}}} \cdot \frac{\partial I_{\text{Conv}}}{\partial Q_{\text{Conv}}} \\ &= \left(\frac{b}{I_R} + 2c \frac{I_{\text{Conv}}}{I_R} \right) S_{\text{Conv}} \cdot \frac{Q_{\text{Conv}}}{V_{\text{Conv}} \sqrt{P_{\text{Conv}}^2 + Q_{\text{Conv}}^2}} \end{aligned} \quad (13)$$

The total system power losses can be calculated by,

$$P_{\text{LOSS}} = P_{\text{Grid}}^{\text{LOSS}} + P_{\text{WfVSC}}^{\text{LOSS}} + \sum_{i=1}^{N_W} P_{\text{GSC}_i}^{\text{LOSS}}, \quad (14)$$

C. Var Limit Sensitivity of WTGs

For a full-scale converter WTG, the Var capability limit $[Q_W^{\min}, Q_W^{\max}]$ depends on its active power output and terminal

voltage. In this paper, a look-up table of the PQ capacity curve is used and the sensitivity coefficients are approximately calculated using the linear interpolation method [31].

IV. PREDICTIVE MODELING

In this section, the predictive models of WfVSC and WTGs are presented which are used for the MPC.

A. Modeling of WTGs

For a full-scale converter WTG, the control of active and reactive power is decoupled by the full-scale converter. Suppose the active and reactive power references and current measurements of the WTG are P_W^{ref} , Q_W^{ref} , $P_W(t_0)$ and $Q_W(t_0)$ where t_0 is the current time, $\Delta P_W^{\text{ref}} = P_W^{\text{ref}} - P_W(t_0)$ and $\Delta Q_W^{\text{ref}} = Q_W^{\text{ref}} - Q_W(t_0)$. Considering the effects of time delay of the communication system and dynamic response of the WTG control system, the dynamic behavior of the power control loops of WTGs could be described by a first-order lag function [13], [15],

$$\Delta P_W = \frac{1}{1 + sT_W^P} \Delta P_W^{\text{ref}} \quad (15)$$

$$\Delta Q_W = \frac{1}{1 + sT_W^Q} \Delta Q_W^{\text{ref}} \quad (16)$$

where T_W^P and T_W^Q are the time constants, which are in the range of 1~10 s [34]. Accordingly, the continuous state space of a wind farm with N_W WTGs can be formulated as,

$$\Delta \dot{P}_W = A_W^P \Delta P_W + B_W^P \Delta P_W^{\text{ref}}, \quad (17)$$

$$\Delta \dot{Q}_W = A_W^Q \Delta Q_W + B_W^Q \Delta Q_W^{\text{ref}}, \quad (18)$$

where

$$\begin{aligned} \Delta P_W &= [\Delta P_{W_1}, \Delta P_{W_2}, \dots, \Delta P_{W_{N_W}}]^T, \\ \Delta P_W^{\text{ref}} &= [\Delta P_{W_1}^{\text{ref}}, \Delta P_{W_2}^{\text{ref}}, \dots, \Delta P_{W_{N_W}}^{\text{ref}}]^T, \\ \Delta Q_W &= [\Delta Q_{W_1}, \Delta Q_{W_2}, \dots, \Delta Q_{W_{N_W}}]^T, \\ \Delta Q_W^{\text{ref}} &= [\Delta Q_{W_1}^{\text{ref}}, \Delta Q_{W_2}^{\text{ref}}, \dots, \Delta Q_{W_{N_W}}^{\text{ref}}]^T, \\ A_W^P &= \text{diag}(-1/T_{W_1}^P, -1/T_{W_2}^P, \dots, -1/T_{W_{N_W}}^P), \\ B_W^P &= \text{diag}(1/T_{W_1}^P, 1/T_{W_2}^P, \dots, 1/T_{W_{N_W}}^P), \\ A_W^Q &= \text{diag}(-1/T_{W_1}^Q, -1/T_{W_2}^Q, \dots, -1/T_{W_{N_W}}^Q), \\ B_W^Q &= \text{diag}(1/T_{W_1}^Q, 1/T_{W_2}^Q, \dots, 1/T_{W_{N_W}}^Q). \end{aligned}$$

B. Modeling of WfVSC

The structure of WfVSC station with a standard cascaded control structure, i.e., inner current control loop and outer control loop, is illustrated in Fig. 3. The control strategy of the outer loop is the AC voltage magnitude control which is often adopted in OWF integration. The phase reactor and converter transformer are represented together by $Z_c = R_c + j\omega L_c$. The

mathematical model of the system in the synchronized rotating dq reference frame is,

$$L_c \frac{di_c^d}{dt} = -R_c i_c^d + \omega L_c i_c^q + u_s^d - u_c^d, \quad (19a)$$

$$L_c \frac{di_c^q}{dt} = -R_c i_c^q + \omega L_c i_c^d + u_s^q - u_c^q, \quad (19b)$$

$$C_f \frac{du_s^d}{dt} = i_s^d - i_c^d + \omega C_f u_s^q, \quad (20a)$$

$$C_f \frac{du_s^q}{dt} = i_s^q - i_c^q - \omega C_f u_s^d. \quad (20b)$$

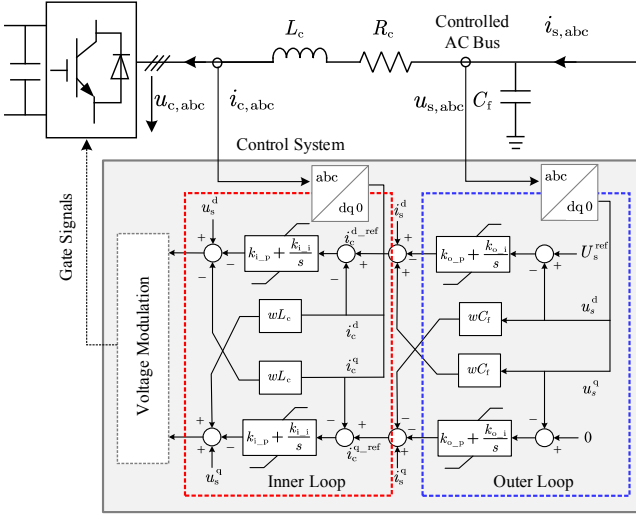


Fig. 3. Cascaded control structure of WFVSC.

The whole system comprised of the physical model of VSC and control system can be decoupled in the dq frame through the decoupling terms ($\Delta u_c^d = \omega L_c i_c^q$, $\Delta u_c^q = -\omega L_c i_c^d$ for the inner loop and $\Delta i_s^d = \omega C_f u_s^q$, $\Delta i_s^q = -\omega C_f u_s^d$ for the outer loop). According to the control strategy, the disturbance in the q-axis can be neglected, i.e., $U_s = \sqrt{(u_s^d)^2 + (u_s^q)^2} \approx u_s^d$ [35]. And the control performance of the inner loop can be improved by selecting suitable parameters of the PI controller, which can be determined by,

$$k_{i_p} = \frac{L_c}{T_{inr}}, \quad (21a)$$

$$k_{i_i} = \frac{R_c}{T_{inr}} \quad (21b)$$

where k_{i_p} and k_{i_i} are the proportional and integral gains of the PI controllers of the inner loop, respectively. T_{inr} is the desired closed loop time constant for the inner current control loop. Generally, T_{inr} is chosen between 5~10 times slower than the switching frequency. Considering the fast dynamic response capability of the inner control loop, the disturbances of i_s^d and u_s^q are approximately compensated by the compensating terms. Thus, the WFVSC system model can be

simplified as shown in Fig. 4. The time delay can be modelled by a first-order lag function with a time constant of T_d .

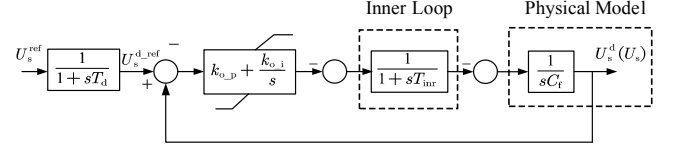


Fig. 4. AC voltage control loop of the WFVSC.

Introducing a state variable Δi_{PI}^d , the state space model of WFVSC can be described by,

$$\Delta u_s^{d_ref} = \frac{1}{1+sT_d} \Delta U_s^{ref}, \quad (22a)$$

$$\Delta u_s^d = -\frac{1}{sC_f} \Delta i_{PI}^d, \quad (22b)$$

$$\Delta u_{int}^d = \frac{\Delta u_s^{d_ref} - \Delta u_s^d}{s}, \quad (22c)$$

$$\Delta i_{PI}^d = -\frac{1}{1+sT_{inr}} \left(k_{o_p} + \frac{k_{o_i}}{s} \right) (\Delta u_s^{d_ref} - \Delta u_s^d), \quad (22d)$$

with

$$\Delta U_s = U_s - U_s(t_0),$$

$$\Delta U_c = U_c - U_c(t_0),$$

$$\Delta u_s^{d_ref} = u_s^{d_ref} - u_s^{d_ref}(t_0),$$

$$\Delta u_s^d = u_s^d - u_s^d(t_0),$$

$$\Delta u_{int}^d = \frac{u_s^{d_ref} - u_s^d}{s},$$

where U_s^{ref} and U_s are the voltage reference from the MPC controller and voltage of POC, respectively; U_c is the voltage at the VSC terminal; s denotes the complex variable; k_{o_p} and k_{o_i} are the proportional and integral gains of the PI controllers of the outer control loop, respectively.

Represent the state space by a matrix form,

$$\Delta \dot{x}_C = A_C \Delta x_C + B_C \Delta u_C, \quad (23)$$

where

$$\Delta x_C = [\Delta u_s^{d_ref}, \Delta u_s^d, \Delta u_{int}^d, \Delta i_{PI}^d]^T, \Delta u_C = [\Delta U_s^{ref}],$$

$$A_C = \begin{bmatrix} -\frac{1}{T_d} & 0 & 0 & 0 \\ 0 & 0 & 0 & \frac{1}{C_f} \\ 1 & -1 & 0 & 0 \\ -\frac{k_{o_p}}{T_{inr}} & \frac{k_{o_p}}{T_{inr}} & -\frac{k_{o_i}}{T_{inr}} & -\frac{1}{T_{inr}} \end{bmatrix}, B_C = \begin{bmatrix} \frac{1}{T_d} \\ 0 \\ 0 \\ 0 \end{bmatrix}.$$

C. Modeling of the Whole System

For the phasor analysis presented in following sections, the VSC can be regarded as a slack bus of the offshore AC grid (i.e. $\bar{V}_C = V_C e^{j0}$) and $\bar{V}_S = V_S e^{j\theta_S}$ denotes the voltage at the

controlled AC bus. V_s and V_c are equal to U_s and U_c in per unit, respectively. To predict the changes of voltages in the grid, the slack bus voltage should be predicted firstly. Due to the fast tracking capability of the control system of the VSC, the d-axis voltage u_s^d can quickly track the reference U_s^{ref} . The controlled AC bus voltage \bar{V}_s can be affected by the converter terminal voltage \bar{V}_c and the WTGs power outputs. Assuming the sensitivity coefficients are constant during the prediction horizon, a linearized model around the operating point is used to predict the voltage changes, which is expressed as,

$$\Delta V_s \approx \frac{\partial V_s}{\partial P_w} \Delta P_w + \frac{\partial V_s}{\partial Q_w} \Delta Q_w + \frac{\partial V_s}{\partial V_c} \Delta V_c, \quad (24)$$

where $\partial V_s / \partial P_w$, $\partial V_s / \partial Q_w$ and $\partial V_s / \partial V_c$ are the sensitivity coefficients. Then, ΔV_c can be inversely derived using (24).

So far, the continuous state space model of the whole system comprised of N_w WTGs and a WFVSC can be formulated as,

$$\begin{aligned} \Delta \dot{x} &= A \Delta x + B \Delta u \\ \Delta y &= C \Delta x \end{aligned} \quad (25)$$

where

$$\Delta x = [\Delta x_1, \Delta x_2, \dots, \Delta x_{N_x}]^T = \underbrace{[\Delta u_s^{\text{d,ref}}, \Delta u_s^{\text{d}}, \Delta u_{\text{int}}^{\text{d}}, \Delta i_{\text{d}}^{\text{PI}}]}_{\Delta x_c}, \underbrace{[\Delta P_{w_1}, \Delta P_{w_2}, \dots, \Delta P_{w_{N_w}}, \Delta Q_{w_1}, \Delta Q_{w_2}, \dots, \Delta Q_{w_{N_w}}]}_{\Delta Q_w}^T,$$

$$\begin{aligned} \Delta u &= [\Delta u_1, \Delta u_2, \dots, \Delta u_{N_u}]^T \\ &= [\Delta V_s^{\text{ref}}, \Delta P_{w_1}^{\text{ref}}, \dots, \Delta P_{w_{N_w}}^{\text{ref}}, \Delta Q_{w_1}^{\text{ref}}, \dots, \Delta Q_{w_{N_w}}^{\text{ref}}]^T, \end{aligned}$$

$$\begin{aligned} \Delta y &= [\Delta y_1, \Delta y_2, \dots, \Delta y_{N_y}]^T \\ &= [\Delta V_c, \Delta P_{w_1}, \dots, \Delta P_{w_{N_w}}, \Delta Q_{w_1}, \dots, \Delta Q_{w_{N_w}}]^T, \end{aligned}$$

$$A = \begin{bmatrix} A_c & & \\ & A_w^P & \\ & & A_w^Q \end{bmatrix}, B = \begin{bmatrix} B_c & & \\ & B_w^P & \\ & & B_w^Q \end{bmatrix},$$

$$C = \begin{bmatrix} C_1 & C_2 & C_3 \\ & C_4 & \\ & & C_5 \end{bmatrix},$$

with

$$C_1 = - \left(\frac{\partial V_s}{\partial V_c} \right)^{-1} [0, -1, 0, 0], C_4 = C_5 = I_{N_w},$$

$$C_2 = - \left(\frac{\partial V_s}{\partial V_c} \right)^{-1} \left[\frac{\partial V_s}{\partial P_{w_1}}, \frac{\partial V_s}{\partial P_{w_2}}, \dots, \frac{\partial V_s}{\partial P_{w_{N_w}}} \right]$$

$$C_3 = - \left(\frac{\partial V_s}{\partial V_c} \right)^{-1} \left[\frac{\partial V_s}{\partial Q_{w_1}}, \frac{\partial V_s}{\partial Q_{w_2}}, \dots, \frac{\partial V_s}{\partial Q_{w_{N_w}}} \right]$$

Based on the continuous time model, the discrete time state space model with sampling time ΔT_p can be expressed as,

$$\begin{aligned} \Delta x(k+1) &= G \Delta x(k) + H \Delta u(k) \\ \Delta y(k) &= C \Delta x(k) \end{aligned} \quad (26)$$

where

$$G = e^{A \Delta T_p}, H = \int_0^{\Delta T_p} e^{A \tau} B d\tau.$$

V. FORMULATION OF MPC BASED ENHANCED VOLTAGE CONTROL

In this section, the mathematical formulation of the MPC based EVCS for OWFs is presented. The main objective of the EVCS is to track the power reference given by TSOs and maintain the terminal voltages all WTGs within the specified limits. Moreover, the economical operation is taken into consideration. Consequently, two control modes are designed for different operating conditions.

A. MPC Principle

MPC is a widely used control method. In MPC, the control input is obtained by solving a discrete-time optimal control problem over a given horizon. An optimal control input sequence is produced and only the first control in the sequence is applied [32].

The principle of MPC used in this paper is graphically illustrated in Fig. 5. For wind farm voltage control, T_c is normally in seconds, which is large than the fast Var devices. To capture the fast dynamics of the system, the sampling time ΔT_p should be smaller than the control period T_c . The suitable prediction horizon T_p is determined by the dynamic performance of the control system. The performance of MPC heavily depends on the selection of T_p . If T_p is too large, the accuracy of sensitivity coefficients might decrease and the computational burdens will be increased. If T_p is too small, dynamics cannot be well coordinated [13].

For a prediction horizon, the total control steps, number of prediction steps within one control period and total prediction steps are $N_c = T_p / T_c$, $N_s = T_c / \Delta T_p$ and $N_p = T_p / \Delta T_p$, respectively. The control actions are only changed at the beginning of the control period and maintained within the control period.

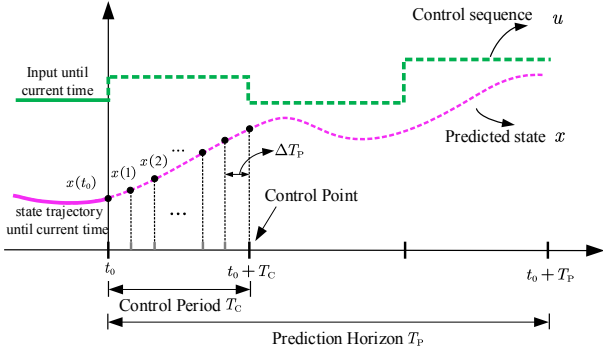


Fig. 5 Principle of MPC.

B. Cost Function

The cost functions of the two control modes are presented as follows.

a. Normal mode

If the terminal voltages of all WTGs and MV bus voltages are within its feasible range, i.e., $\|V_W - V_W^{\text{ref}}\| < V_W^{\text{th}}$ and $\|V_{\text{MV}} - V_{\text{MV}}^{\text{ref}}\| < V_{\text{MV}}^{\text{th}}$, the control system will operate in the normal mode. V_W^{ref} and $V_{\text{MV}}^{\text{ref}}$ are the nominal voltage (typically 1.0 p.u.). V_W^{th} and $V_{\text{MV}}^{\text{th}}$ refer to the threshold value. The voltages, power losses and active power distribution are optimized in this mode.

1) *Objective 1*: The first objective is voltage regulation. According to the theorem in [36], the OWF presented in Fig. 1 can be divided into several subzones for voltage regulation. Two radial feeders with a common root MV bus can be regarded as an isolate voltage regulation zone. The MV root buses (MV_1~MV_4 in Fig. 1) can be considered as the pilot buses of the subzones. Since the voltage of pilot bus can reflect the voltage conditions of the subzone, in the normal mode, the cost function of voltage regulation in MPC can be described by,

$$\text{Obj}_V = \sum_{k=1}^{N_p} \|\Delta V_{\text{MV}}^{\text{pre}}(k)\|^2 \quad (27)$$

with

$$\Delta V_{\text{MV}}^{\text{pre}} = [\Delta V_{\text{MV}_1}^{\text{pre}}, \Delta V_{\text{MV}_2}^{\text{pre}}, \dots, \Delta V_{\text{MV}_{N_{\text{MV}}}}^{\text{pre}}]^T,$$

where $\Delta V_{\text{MV}_i}^{\text{pre}}$ is the predictive value of voltage deviation of bus MV_ $_i$ to its reference value $V_{\text{MV}}^{\text{ref}}$, and N_{MV} is the total number of MV buses. Since the WTGs and VSC can affect voltage deviations of MV buses, the predictive value $\Delta V_{\text{MV}_i}^{\text{pre}}$ can be calculated by,

$$\begin{aligned} \Delta V_{\text{MV}_i}^{\text{pre}}(k) = & V_{\text{MV}_i}(t_0) + \frac{\partial V_{\text{MV}_i}}{\partial P_W} \Delta P_W(k) \\ & + \frac{\partial V_{\text{MV}_i}}{\partial Q_W} \Delta Q_W(k) + \frac{\partial V_{\text{MV}_i}}{\partial V_C} \Delta V_C(k) - V_{\text{MV}}^{\text{ref}} \end{aligned} \quad (28)$$

where $V_{\text{MV}_i}(t_0)$ is the measurement of i -th MV bus voltage at current time t_0 .

2) *Objective 2*: Secondly, the active power losses are optimized in this mode, i.e.,

$$\text{Obj}_L = \sum_{k=1}^{N_p} \|P_{\text{LOSS}}^{\text{pre}}(k)\|^2. \quad (29)$$

The predictive value of active power losses can be calculated by,

$$\begin{aligned} P_{\text{LOSS}}^{\text{pre}}(k) = & \frac{\partial P_{\text{LOSS}}}{\partial P_W} \Delta P_W(k) + \frac{\partial P_{\text{LOSS}}}{\partial Q_W} \Delta Q_W(k) \\ & + \frac{\partial P_{\text{LOSS}}}{\partial V_C} \Delta V_C(k) + P_{\text{LOSS}}^{\text{pre}}(t_0), \end{aligned} \quad (30)$$

where $V = [V_1, V_2, \dots, V_N]^T$, $\theta = [\theta_1, \theta_2, \dots, \theta_N]^T$ and the sensitivity matrix is presented in Appendix B.

3) *Objective 3*: Thirdly, considering the active power dispatch based on the PD strategy has the advantage of taking into consideration the maximum available power of WTGs while also optimizing the Var capacity of each WTG, the active power of each WTG shall be dispatched as close as possible to its PD based reference. Thus, the third cost function can be described by,

$$\text{Obj}_P = \sum_{k=1}^{N_p} \|\Delta P_W^{\text{PD}}(k)\|^2. \quad (31)$$

The predictive value ΔP_W^{PD} can be calculated by

$$\Delta P_W^{\text{PD}}(k) = P_W(t_0) + \Delta P_W(k) - P_W^{\text{PD-ref}}, \quad (32)$$

where $P_W^{\text{PD-ref}} = [P_{W_1}^{\text{PD-ref}}, P_{W_2}^{\text{PD-ref}}, \dots, P_{W_{N_W}}^{\text{PD-ref}}]$.

According to (27), (29) and (31), the cost function of normal mode can be expressed by,

$$\min (\lambda_V \text{Obj}_V + \lambda_L \text{Obj}_L + \lambda_P \text{Obj}_P), \quad (33)$$

where λ_V, λ_L and λ_P are the weighting coefficients for Obj_V , Obj_L and Obj_P , respectively.

b. Corrective mode

The corrective mode is designed as a back-up mode. If any voltage violates the threshold, the control system will switch to the corrective mode. In this mode, only the voltages are considered as control objective. Define $\Delta V_W^{\text{pre}} = [\Delta V_{W_1}^{\text{pre}}, \Delta V_{W_2}^{\text{pre}}, \dots, \Delta V_{W_{N_W}}^{\text{pre}}]^T$, the cost function is,

$$\min \sum_{k=1}^{N_p} (\|\Delta V_W^{\text{pre}}(k)\|_{\lambda_W}^2 + \|\Delta V_{\text{MV}}^{\text{pre}}(k)\|_{\lambda_{\text{MV}}}^2) \quad (34)$$

where $\lambda_W = \text{diag}(\lambda_{W_1}, \lambda_{W_2}, \dots, \lambda_{W_{N_W}})$ and $\lambda_{\text{MV}} = \text{diag}(\lambda_{\text{MV}_1}, \lambda_{\text{MV}_2}, \dots, \lambda_{\text{MV}_{N_{\text{MV}}}})$ denote the weighting coefficient matrices. The predictive voltage deviations to its reference V_W^{ref} can be calculated by,

$$\begin{aligned} \Delta V_{W_i}^{\text{pre}}(k) = & V_{W_i}(t_0) + \frac{\partial V_{W_i}}{\partial P_W} \Delta P_W(k) \\ & + \frac{\partial V_{W_i}}{\partial Q_W} \Delta Q_W(k) + \frac{\partial V_{W_i}}{\partial V_C} \Delta V_C(k) - V_W^{\text{ref}} \end{aligned} \quad (35)$$

In order to correct the voltages efficiently, the weighting coefficients are determined through a dynamic allocation approach according to the degree of voltage deviations with a

deadband, as illustrated in Fig. 6. When the absolute value of voltage deviation is less than 0.01 p.u., the weighting factor is set as zero. Once it exceeds 0.01 p.u., the weighting factor is linear with respect to the voltage deviation value. Compared with the normal mode, the WTGs and WFVSC can be fully optimized to contribute to voltage regulation in this mode.

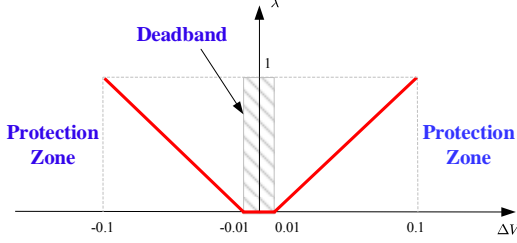


Fig. 6 Dynamic weighting coefficients.

C. Constraints

1) *WTG Constraints*: The active and reactive power of WTGs are constrained as follows,

$$\begin{aligned} 0 &\leq P_{W_i}(k) \leq P_{W_i}^{av}, \\ Q_{W_i}^{\min}(k) &\leq Q_{W_i}(k) \leq Q_{W_i}^{\max}(k), \\ i &= 1, 2, \dots, N_W, \quad k = 1, 2, \dots, N_P. \end{aligned} \quad (36)$$

where $P_{W_i}^{av}$ is the available wind power, $Q_{W_i}^{\min}(k)$ and $Q_{W_i}^{\max}(k)$ are the minimum and maximum Var capacity of WTGs, respectively. $Q_{W_i}^{\min}(k)$ and $Q_{W_i}^{\max}(k)$ are affected by the terminal voltage magnitude and active power output of the WTG, which can be predicted based on a linearized method,

$$Q_{W_i}^{\min}(k) \approx Q_{W_i}^{\min}(t_0) + \frac{\partial Q_{W_i}^{\min}}{\partial P_W} \Delta P_{W_i}(k) + \frac{\partial Q_{W_i}^{\min}}{\partial V_W} \Delta V_{W_i}(k), \quad (37a)$$

$$Q_{W_i}^{\max}(k) \approx Q_{W_i}^{\max}(t_0) + \frac{\partial Q_{W_i}^{\max}}{\partial P_W} \Delta P_{W_i}(k) + \frac{\partial Q_{W_i}^{\max}}{\partial V_W} \Delta V_{W_i}(k), \quad (37b)$$

where

$$\Delta V_{W_i}(k) = \frac{\partial V_{W_i}}{\partial P_W} \Delta P_W + \frac{\partial V_{W_i}}{\partial Q_W} \Delta Q_W + \frac{\partial V_{W_i}}{\partial V_C} \Delta V_C$$

As mentioned in Section III, the sensitivity coefficients $\partial Q_{W_i}^{\min}/\partial V_W$, $\partial Q_{W_i}^{\min}/\partial P_W$, $\partial Q_{W_i}^{\max}/\partial V_W$ and $\partial Q_{W_i}^{\max}/\partial P_W$ are calculated based on the linear interpolation approach.

2) *VSC Constraints*: Since the AC voltage control is adopted by the local controller of WFVSC, the voltage reference at the controlled AC bus is constrained by,

$$\begin{aligned} V_S^{\min} &\leq \Delta V_S^{\text{ref}}(k) + V_S(t_0) \leq V_S^{\max}, \quad \|\Delta V_S^{\text{ref}}\| < \Delta V_S^{\max}, \\ k &= 1, 2, \dots, N_C \end{aligned} \quad (38)$$

where V_S^{\min} and V_S^{\max} are the minimum and maximum limits of V_S , respectively and ΔV_S^{\max} is the maximum ramp rate.

3) *System Constraints*: The OWF is required to track the power reference P_{WF}^{ref} from system operators, which can be expressed as,

$$\sum_{i=1}^{N_W} P_{W_i}^{\text{ref}} = P_{WF}^{\text{ref}}. \quad (39)$$

The formulated MPC problem (27) ~ (39) can be transformed into a standard quadratic-programming (QP) problem and efficiently solved by commercial QP solvers in milliseconds [37]. More details about the derivations of the mathematical formulation of EVCS-MPC are presented in Appendix A.

VI. CASE STUDY

A VSC-HVDC connected OWF system with 64 WTGs is used to demonstrate the proposed MPC based EVCS in this section. The structure of the system is presented in Section II. The wind field model considering the turbulences and wake effects for the OWF is generated using the SimWindFarm, a toolbox for dynamic wind farm modeling and simulation [38]. The basic electrical and control system parameters are presented in Appendix B.

To examine the control performance of the MPC-EVCS, several control methods are used to make comparisons: 1) optimal control (OPC) [16]; and 2) the voltage control method based on MPC without considering the effects of active power of WTGs in the optimization (MPC-Q).

A. Scenario A: Normal Operation

The total simulation time for this scenario is 600s. Fig. 7 shows the available power and active power reference considering the power ramp rate of the wind farm.

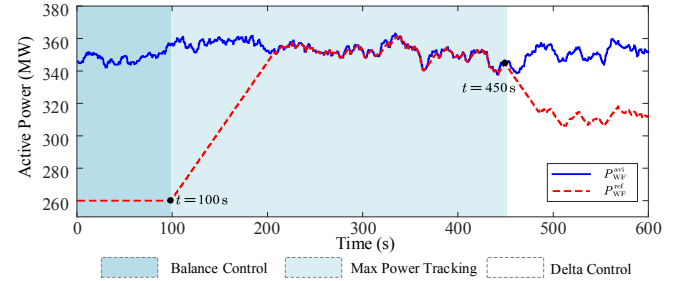


Fig. 7. Active power output of the OWF for Scenario A.

Fig. 8 shows the voltage of bus MV_1 and terminal voltage of WTG_64 (the furthest bus along the feeder). All the three OWF controllers can keep the voltages below their thresholds, and the control systems operate in normal mode. The standard deviations $\sigma(V_{MV_1})$ are 0.8512% for OPC, 0.8387% for MPC-Q and 0.8367% for MPC-EVCS. V_{W_64} is closer to the nominal value using MPC-Q or MPC-EVCS than using OPC and is smoother using MPC-EVCS than using MPC-Q owing to the consideration of effects of active power of WTGs on voltage deviations. Thus, the MPC-EVCS shows better performance for voltage regulation.

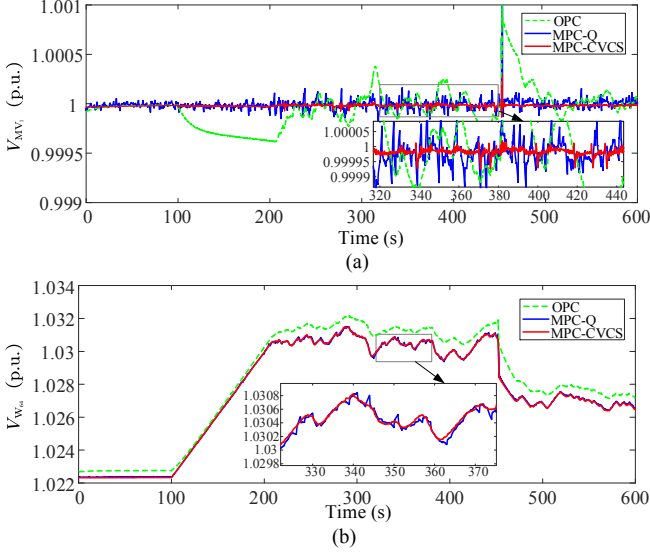


Fig. 8. Voltages of different buses. (a) Voltage of bus MV_1; (b) terminal voltage of WTG_64.

Fig. 9 shows the power losses of the system. The mean values of power losses within the operating time are 19.5154 MW for OPC, 19.3312 MW for MPC-Q and 19.2187 MW for MPC-EVCS, respectively. It can be seen that the MPC-EVCS shows better performance in power losses reduction.

The reactive power output of WTG_1 is illustrated in Fig. 10. The MPC-Q and MPC-EVCS can both regulate the reactive power of WTGs within small ranges, which enlarges the Var reserves. Compared with the MPC-Q, the MPC-EVCS regulates the reactive power outputs of WTGs more smoothly.

Accordingly, all the three controllers show good control performance in normal operation, whereas comparably, the MPC-EVCS is better than the OPC and MPC-Q.

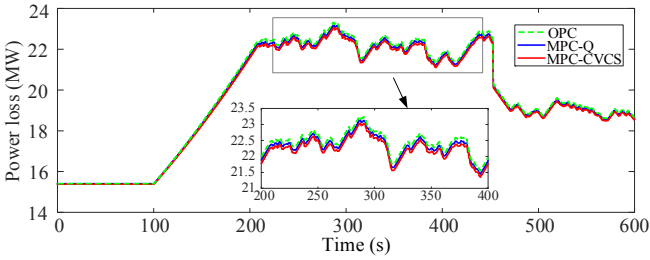


Fig. 9. Power loss of the grid.

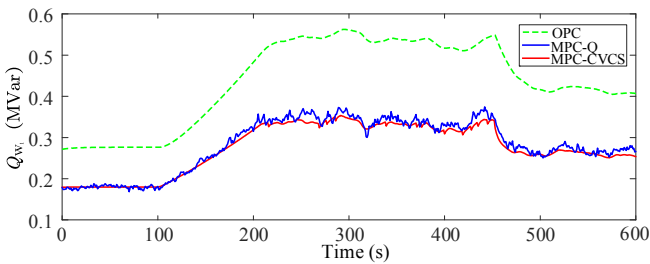


Fig. 10. Reactive power of WTG_1.

B. Scenario B: Voltage Ramp-up Operation

The voltage ramp-up operation of VSC-HVDC connected OWFs is considered for this scenario. In this scenario, the WFVSC builds up the voltage at the beginning. When the terminal voltages of WTGs reach 0.9 p.u., WTGs are connected to the grid and the controller switches to coordinated control strategy (i.e., the OPC, MPC-Q or MPC-EVCS). The total simulation time is 50s. The simulation results are shown in Figs. 11~13.

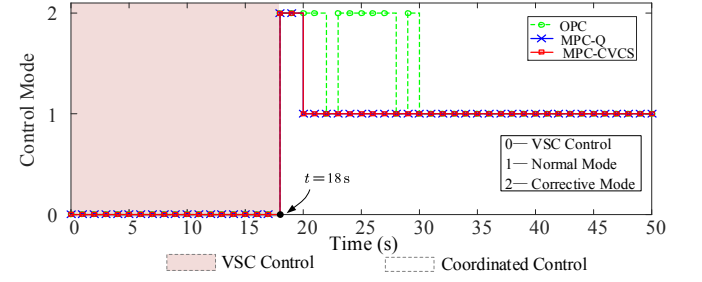


Fig. 11. Control mode switching.

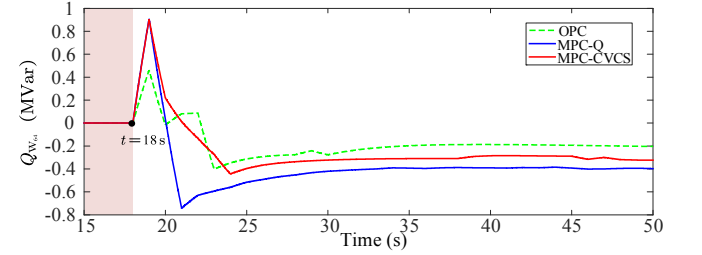


Fig. 12. Reactive power of WTG_64.

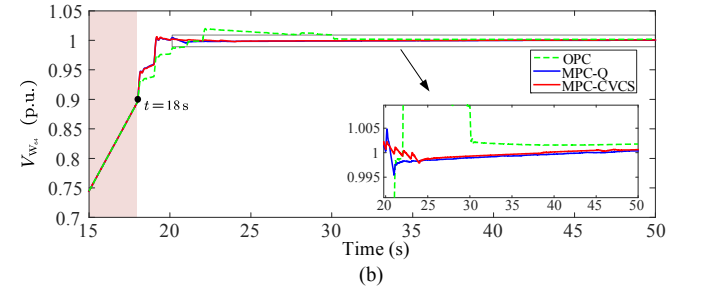
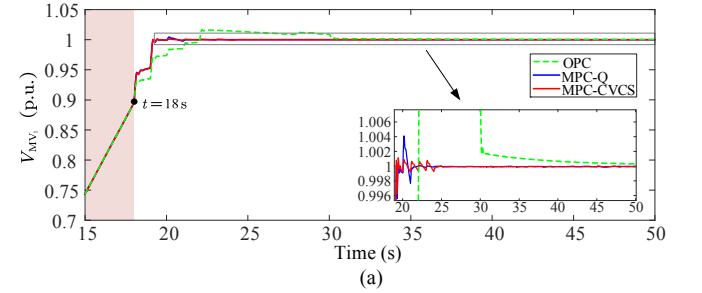


Fig. 13. Voltages of different buses. (a) Voltage of bus MV_1; (b) terminal voltage of WTG_64.

As can be seen from Fig. 11, all the three control methods switch from the VSC control mode to the corrective mode at $t=18$ s. For the MPC-Q and MPC-EVCS, the controllers switch to the normal mode at $t=20$ s and keep stable in the

remaining period. For the OPC, the controller switches between the corrective mode and normal mode for several times during $t = 18 \sim 30$ s and keeps stable after $t = 30$ s. Fig. 12 shows the reactive power of WTG_64. As can be seen, the WTG generates additional reactive power to support the low voltages of the grid at the beginning of the coordinated control. Fig. 13 shows the voltage of bus MV_1 and terminal voltage of WTG_64. It is shown that the three controllers can well regulate the voltages within feasible ranges in seconds. By comparison, the MPC-Q and MPC-EVCS shows better control performance than the OPC, since the voltages recover within the feasible ranges more quickly for the MPC-Q and MPC-EVCS than the OPC.

C. MPC Solver Performance

The time consumed by the solver in MPC should be considered in real-time control. In this study, the QP problem was solved using the interior-point method. The estimated available time to execute the control algorithm can be calculated by $T_C - 2T_d = 800$ ms. The actual mean executing time consumed by the solver in Scenario A is 12.7 ms. Obviously, the actual executing time is much smaller than the available time, satisfying the requirements for real-life application.

VII. CONCLUSIONS

In this paper, a MPC based EVCS is developed to optimize voltage control within VSC-HVDC connected OWFs, which can regulate the voltages while taking into account economical operation of the OWFs. The predictive model of WFVSC with a typical cascaded control structure is derived in details. An analytical sensitivity coefficient calculation method is adopted to improve computational efficiency. In the MPC-EVCS, two control modes are designed for different operating conditions. The case studies show that all the three different optimization control methods OPC, MPC-Q and MPC-EVCS show good control performance in different scenarios. In comparison, the overall performance of the MPC-EVCS is better than the MPC-Q and OPC. Of course, more work is required for further improvement. A nonlinear model of the system will be investigated to more accurately capture the complex dynamics of the systems and improve the control performance in the future work.

APPENDIX A

MATHEMATICAL FORMULATION OF MPC

To derive the mathematical formulation of the optimization problem in the MPC-EVCS, firstly transform the state variables, control variables and output variables into unified forms:

$$\begin{aligned}\Delta U &= [\Delta u(1), \Delta u(2), \dots, \Delta u(N_C)]^T, \\ \Delta X &= [\Delta x(1), \Delta x(2), \dots, \Delta x(N_P)]^T, \\ \Delta Y &= [\Delta y(1), \Delta y(2), \dots, \Delta y(N_P)]^T.\end{aligned}\quad (40)$$

For the sake of clarity, the derivations are divided into four steps as follows.

Step I: Represent ΔX and ΔY by ΔU .

According to (26), it can be obtained that

$$\Delta X = W_{XU} \Delta U \quad (41)$$

$$\Delta Y = W_{YX} \Delta X \quad (42)$$

where

$$W_{XU} = \begin{bmatrix} W_{11} & & & \\ W_{21} & W_{22} & & \\ \vdots & \vdots & \ddots & \\ W_{N_C,1} & W_{N_C,2} & \dots & W_{N_C,N_C} \end{bmatrix}, \quad W_{ij} = \begin{bmatrix} \mathcal{W}_{ij}^1 \\ \mathcal{W}_{ij}^2 \\ \vdots \\ \mathcal{W}_{ij}^{N_S} \end{bmatrix},$$

$$W_{YX} = I_{N_P} \otimes C = \begin{bmatrix} C & & & \\ & C & & \\ & & \ddots & \\ & & & C \end{bmatrix}.$$

The elements of the matrix W_{XU} are calculated using the following recursive method:

For W_{ij} ($i > j$):

$$\mathcal{W}_{ij}^k = G^k \mathcal{W}_{i-1,j}^{N_S}, \quad k = 1, 2, \dots, N_S. \quad (43a)$$

For W_{ij} ($i = j$):

$$\mathcal{W}_{ij}^k = (I + G + G^2 + \dots + G^{k-1})H, \quad k = 1, 2, \dots, N_S. \quad (43b)$$

Step II: Represent the predictive values by ΔU .

Based on (29), $\Delta V_{MV}^{\text{pre}}$ can be transformed into a compact form

$$\Delta V_{MV}^{\text{pre}} = (I_{N_P} \otimes S_{MV}) \Delta Y + \mathbf{1}_{N_P} \otimes (V_{MV}(t_0) - V_{MV}^{\text{ref}}), \quad (44)$$

where

$$S_{MV} = \begin{bmatrix} \frac{\partial V_{MV_1}}{\partial y_1} & \frac{\partial V_{MV_1}}{\partial y_2} & \dots & \frac{\partial V_{MV_1}}{\partial y_{N_y}} \\ \frac{\partial V_{MV_2}}{\partial y_1} & \frac{\partial V_{MV_2}}{\partial y_2} & \dots & \frac{\partial V_{MV_2}}{\partial y_{N_y}} \\ \vdots & \vdots & \ddots & \vdots \\ \frac{\partial V_{MV_{N_{MV}}}}{\partial y_1} & \frac{\partial V_{MV_{N_{MV}}}}{\partial y_2} & \dots & \frac{\partial V_{MV_{N_{MV}}}}{\partial y_{N_y}} \end{bmatrix},$$

which can be directly obtained using (4)~(7).

Similarly, according to (36), ΔV_W^{pre} can be written as

$$\Delta V_W^{\text{pre}} = (I_{N_P} \otimes S_{WT}) \Delta Y + \mathbf{1}_{N_P} \otimes (V_W(t_0) - V_W^{\text{ref}}) \quad (45)$$

where

$$S_{\text{WT}} = \begin{bmatrix} \frac{\partial V_{W_1}}{\partial y_1} & \frac{\partial V_{W_1}}{\partial y_2} & \cdots & \frac{\partial V_{W_1}}{\partial y_{N_y}} \\ \frac{\partial V_{W_2}}{\partial y_1} & \frac{\partial V_{W_2}}{\partial y_2} & \cdots & \frac{\partial V_{W_2}}{\partial y_{N_y}} \\ \vdots & \vdots & \ddots & \vdots \\ \frac{\partial V_{W_{N_w}}}{\partial y_1} & \frac{\partial V_{W_{N_w}}}{\partial y_2} & \cdots & \frac{\partial V_{W_{N_w}}}{\partial y_{N_y}} \end{bmatrix}.$$

Similarly, S_{WT} can be directly calculated using (4)-(7).

According to (31), $P_{\text{LOSS}}^{\text{pre}}$ can be represented by,

$$P_{\text{LOSS}}^{\text{pre}} = (I_{N_p} \otimes S_{\text{PL}}) \Delta Y + \mathbf{1}_{N_p} \otimes P_{\text{LOSS}}(t_0) \quad (46)$$

where

$$S_{\text{PL}} = \begin{bmatrix} \frac{\partial P_{\text{LOSS}}}{\partial y_1}, \frac{\partial P_{\text{LOSS}}}{\partial y_2}, \dots, \frac{\partial P_{\text{LOSS}}}{\partial y_{N_y}} \end{bmatrix}.$$

The calculation of S_{PL} is presented as follows.

From (14), one can obtain,

$$\Delta P_{\text{LOSS}} = \Delta P_{\text{Grid}}^{\text{LOSS}} + \Delta P_{\text{WFVSC}}^{\text{LOSS}} + \Delta \left(\sum_{i=1}^{N_w} P_{\text{GSC}_i}^{\text{LOSS}} \right), \quad (47)$$

where

$$\Delta P_{\text{Grid}}^{\text{LOSS}} = \frac{\partial P_{\text{Grid}}^{\text{LOSS}}}{\partial P_{\text{W}}} \Delta P_{\text{W}} + \frac{\partial P_{\text{Grid}}^{\text{LOSS}}}{\partial Q_{\text{W}}} \Delta Q_{\text{W}} + \frac{\partial P_{\text{Grid}}^{\text{LOSS}}}{\partial V_{\text{C}}} \Delta V_{\text{C}},$$

$$\begin{aligned} \Delta P_{\text{WFVSC}}^{\text{LOSS}} &= \frac{\partial P_{\text{WFVSC}}^{\text{LOSS}}}{\partial P_{\text{WFVSC}}} \Delta P_{\text{WFVSC}} + \frac{\partial P_{\text{Grid}}^{\text{LOSS}}}{\partial Q_{\text{WFVSC}}} \Delta Q_{\text{WFVSC}} \\ &\approx \frac{\partial P_{\text{WFVSC}}^{\text{LOSS}}}{\partial P_{\text{WFVSC}}} (\mathbf{1}_{N_w}^T \Delta P_{\text{W}}) + \frac{\partial P_{\text{WFVSC}}^{\text{LOSS}}}{\partial Q_{\text{WFVSC}}} (\mathbf{1}_{N_w}^T \Delta Q_{\text{W}}), \end{aligned}$$

$$\Delta \left(\sum_{i=1}^{N_w} P_{\text{GSC}_i}^{\text{LOSS}} \right) = \frac{\partial P_{\text{GSC}}^{\text{LOSS}}}{\partial P_{\text{W}}} \Delta P_{\text{W}} + \frac{\partial P_{\text{GSC}}^{\text{LOSS}}}{\partial Q_{\text{GSC}}} \Delta Q_{\text{W}}.$$

Then, S_{PL} can be represented as,

$$S_{\text{PL}} = \begin{bmatrix} \frac{\partial P_{\text{Grid}}^{\text{LOSS}}}{\partial V_{\text{C}}}, \frac{\partial P_{\text{Grid}}^{\text{LOSS}}}{\partial P_{\text{W}}} + \frac{\partial P_{\text{WFVSC}}^{\text{LOSS}}}{\partial P_{\text{WFVSC}}} \cdot \mathbf{1}_{N_w}^T + \frac{\partial P_{\text{GSC}}^{\text{LOSS}}}{\partial P_{\text{GSC}}}, \\ \frac{\partial P_{\text{Grid}}^{\text{LOSS}}}{\partial Q_{\text{W}}} + \frac{\partial P_{\text{WFVSC}}^{\text{LOSS}}}{\partial Q_{\text{WFVSC}}} \cdot \mathbf{1}_{N_w}^T + \frac{\partial Q_{\text{GSC}}^{\text{LOSS}}}{\partial Q_{\text{GSC}}} \end{bmatrix} \quad (48)$$

According to (32), $\Delta P_{\text{W}}^{\text{PD}}$ can be represented by,

$$\Delta P_{\text{W}}^{\text{PD}} = (I_{N_p} \otimes S_{\text{AP}}) \Delta Y + \mathbf{1}_{N_p} \otimes (P_{\text{W}}(t_0) - P_{\text{W}}^{\text{PD-ref}}) \quad (49)$$

where

$$\begin{aligned} S_{\text{AP}} &= \begin{bmatrix} 0 & 1 & 0 & \cdots & 0 & 0 & 0 & \cdots & 0 \\ 0 & 0 & 1 & \cdots & 0 & 0 & 0 & \cdots & 0 \\ \vdots & \vdots & \vdots & \ddots & \vdots & \vdots & \vdots & \ddots & \vdots \\ 0 & 0 & 0 & \cdots & 1 & 0 & 0 & \cdots & 0 \end{bmatrix} \\ &= [\mathbf{0}_{N_w \times 1} \quad I_{N_w} \quad \mathbf{0}_{N_w \times N_w}] \end{aligned}$$

Then, substituting (41)-(42) into (44)-(46) and (49), the predictive values can be explicitly represented by ΔU ,

$$\Delta V_{\text{MV}}^{\text{pre}} = M_{\text{MV}} \Delta U + E_{\text{MV}}, \quad (50a)$$

$$\Delta V_{\text{W}}^{\text{pre}} = M_{\text{WT}} \Delta U + E_{\text{WT}}, \quad (50b)$$

$$P_{\text{LOSS}}^{\text{pre}} = M_{\text{PL}} \Delta U + E_{\text{PL}}, \quad (50c)$$

$$\Delta P_{\text{W}}^{\text{PD}} = M_{\text{AP}} \Delta U + E_{\text{AP}}, \quad (50d)$$

where

$$M_{\text{MV}} = I_{N_p} \otimes S_{\text{MV}} W_{\text{YX}} W_{\text{XU}}, \quad E_{\text{MV}} = \mathbf{1}_{N_p} \otimes (V_{\text{MV}}(t_0) - V_{\text{MV}}^{\text{ref}}),$$

$$M_{\text{WT}} = I_{N_p} \otimes S_{\text{WT}} W_{\text{YX}} W_{\text{XU}}, \quad E_{\text{WT}} = \mathbf{1}_{N_p} \otimes (V_{\text{W}}(t_0) - V_{\text{W}}^{\text{ref}}),$$

$$M_{\text{PL}} = I_{N_p} \otimes S_{\text{PL}} W_{\text{YX}} W_{\text{XU}}, \quad E_{\text{PL}} = \mathbf{1}_{N_p} \otimes P_{\text{LOSS}}(t_0),$$

$$M_{\text{AP}} = I_{N_p} \otimes S_{\text{AP}} W_{\text{YX}} W_{\text{XU}}, \quad E_{\text{AP}} = \mathbf{1}_{N_p} \otimes (P_{\text{W}}(t_0) - P_{\text{W}}^{\text{PD-ref}}).$$

Step III: Represent the constraints by ΔU .

The constraints (36) and (37) can be written compactly as,

$$0 \leq (I_{N_p} \otimes S_{\text{AP}}) \Delta Y + \mathbf{1}_{N_p} \otimes P_{\text{W}}(t_0) \leq \mathbf{1}_{N_p} \otimes P_{\text{W}}^{\text{av}}, \quad (51a)$$

$$Q_{\text{W}}^{\text{min}} \leq (I_{N_p} \otimes S_{\text{RP}}) \Delta Y + \mathbf{1}_{N_p} \otimes Q_{\text{W}}(t_0) \leq Q_{\text{W}}^{\text{max}}. \quad (51b)$$

where

$$\begin{aligned} S_{\text{RP}} &= \begin{bmatrix} 0 & 0 & 0 & \cdots & 0 & 1 & 0 & \cdots & 0 \\ 0 & 0 & 0 & \cdots & 0 & 0 & 1 & \cdots & 0 \\ \vdots & \vdots & \vdots & \ddots & \vdots & \vdots & \vdots & \ddots & \vdots \\ 0 & 0 & 0 & \cdots & 0 & 0 & 0 & \cdots & 1 \end{bmatrix} \\ &= [\mathbf{0}_{N_w \times 1} \quad \mathbf{0}_{N_w \times N_w} \quad I_{N_w}] \end{aligned}$$

$$Q_{\text{W}}^{\text{min}} = I_{N_p} \otimes (S_{Q_{\text{min}}}^P S_{\text{AP}} + S_{Q_{\text{min}}}^V S_{\text{MV}}) \Delta Y + \mathbf{1}_{N_p} \otimes Q_{\text{W}}^{\text{min}}(t_0)$$

$$Q_{\text{W}}^{\text{max}} = I_{N_p} \otimes (S_{Q_{\text{max}}}^P S_{\text{AP}} + S_{Q_{\text{max}}}^V S_{\text{MV}}) \Delta Y + \mathbf{1}_{N_p} \otimes Q_{\text{W}}^{\text{max}}(t_0)$$

with

$$S_{Q_{\text{min}}}^P = \text{diag} \left(\frac{\partial Q_{W_1}^{\text{min}}}{\partial P_{W_1}}, \frac{\partial Q_{W_2}^{\text{min}}}{\partial P_{W_2}}, \dots, \frac{\partial Q_{W_{N_w}}^{\text{min}}}{\partial P_{W_{N_w}}} \right),$$

$$S_{Q_{\text{min}}}^V = \text{diag} \left(\frac{\partial Q_{W_1}^{\text{min}}}{\partial V_{W_1}}, \frac{\partial Q_{W_2}^{\text{min}}}{\partial V_{W_2}}, \dots, \frac{\partial Q_{W_{N_w}}^{\text{min}}}{\partial V_{W_{N_w}}} \right),$$

$$S_{Q_{\text{max}}}^P = \text{diag} \left(\frac{\partial Q_{W_1}^{\text{max}}}{\partial P_{W_1}}, \frac{\partial Q_{W_2}^{\text{max}}}{\partial P_{W_2}}, \dots, \frac{\partial Q_{W_{N_w}}^{\text{max}}}{\partial P_{W_{N_w}}} \right),$$

$$S_{Q_{\text{max}}}^V = \text{diag} \left(\frac{\partial Q_{W_1}^{\text{max}}}{\partial V_{W_1}}, \frac{\partial Q_{W_2}^{\text{max}}}{\partial V_{W_2}}, \dots, \frac{\partial Q_{W_{N_w}}^{\text{max}}}{\partial V_{W_{N_w}}} \right).$$

Then, substituting (41)-(42) into (51), (51) can be arranged to

$$\Delta U_P^{\text{min}} \leq F_P \Delta U \leq \Delta U_P^{\text{max}}, \quad (52a)$$

$$\Delta U_Q^{\text{min}} \leq F_Q \Delta U \leq \Delta U_Q^{\text{max}}, \quad (52b)$$

with

$$F_P = (I_{N_p} \otimes S_{AP})W_{YX}W_{XU},$$

$$\Delta U_P^{\min} = -\mathbf{1}_{N_p} \otimes P_W(t_0),$$

$$\Delta U_P^{\max} = \mathbf{1}_{N_p} \otimes P_W^{\text{av}} - \mathbf{1}_{N_p} \otimes P_W(t_0),$$

$$F_{Q_{\min}} = (I_{N_p} \otimes S_{RP})W_{YX}W_{XU} \\ - I_{N_p} \otimes (S_{Q_{\min}}^P S_{AP} + S_{Q_{\min}}^V S_{WT})W_{YX}W_{XU},$$

$$F_{Q_{\max}} = (I_{N_p} \otimes S_{RP})W_{YX}W_{XU} \\ - I_{N_p} \otimes (S_{Q_{\max}}^P S_{AP} + S_{Q_{\max}}^V S_{WT})W_{YX}W_{XU},$$

$$\Delta U_Q^{\min} = \mathbf{1}_{N_p} \otimes Q_W^{\min}(t_0) - \mathbf{1}_{N_p} \otimes Q_W(t_0),$$

$$\Delta U_Q^{\max} = \mathbf{1}_{N_p} \otimes Q_W^{\max}(t_0) - \mathbf{1}_{N_p} \otimes Q_W(t_0).$$

The constraints (38) can be written compactly as,

$$\mathbf{1}_{N_C} \otimes V_S^{\min} \leq (I_{N_C} \otimes S_{VU})\Delta U + \mathbf{1}_{N_C} \otimes V_S(t_0) \leq \mathbf{1}_{N_C} \otimes V_S^{\max}, \quad (53a)$$

$$-\mathbf{1}_{N_C} \otimes \Delta V_S^{\max} \leq (I_{N_C} \otimes S_{VU})\Delta U \leq \mathbf{1}_{N_C} \otimes \Delta V_S^{\max}, \quad (53b)$$

where $S_{VU} = \underbrace{[1, 0, 0, \dots, 0]}_{N_u}$.

Similarly, (53) can be simplified to

$$\Delta U_V^{\min} \leq F_V \Delta U \leq \Delta U_V^{\max}, \quad (54a)$$

$$\Delta U_{\Delta V}^{\min} \leq F_{\Delta V} \Delta U \leq \Delta U_{\Delta V}^{\max}, \quad (54b)$$

where

$$F_V = F_{\Delta V} = I_{N_C} \otimes S_{VU},$$

$$\Delta U_V^{\min} = \mathbf{1}_{N_C} \otimes V_S^{\min} - \mathbf{1}_{N_C} \otimes V_S(t_0),$$

$$\Delta U_V^{\max} = \mathbf{1}_{N_C} \otimes V_S^{\max} - \mathbf{1}_{N_C} \otimes V_S(t_0),$$

$$\Delta U_{\Delta V}^{\min} = -\mathbf{1}_{N_C} \otimes \Delta V_S^{\max},$$

$$\Delta U_{\Delta V}^{\max} = \mathbf{1}_{N_C} \otimes \Delta V_S^{\max}.$$

According to (40), the constraint of active power output of the wind farm can be compactly represented as,

$$F_E \Delta U = \Delta U_E \quad (55)$$

where

$$F_E = \mathbf{1}_{N_C} \otimes \begin{bmatrix} 0 & 1 & 1 & \cdots & 1 & 0 & 0 & \cdots & 0 \\ 0 & 1 & 1 & \cdots & 1 & 0 & 0 & \cdots & 0 \\ \vdots & \vdots & \vdots & \ddots & \vdots & \vdots & \vdots & \ddots & \vdots \\ 0 & 1 & 1 & \cdots & 1 & 0 & 0 & \cdots & 0 \end{bmatrix}$$

$$= \mathbf{1}_{N_C} \otimes \begin{bmatrix} \mathbf{0}_{N_w \times 1} & \mathbf{1}_{N_w}^T & \mathbf{1}_{N_w} & \mathbf{0}_{N_w \times N_w} \end{bmatrix}$$

$$\Delta U_E = \mathbf{1}_{N_C} \otimes (P_{WF}^{\text{ref}} - \mathbf{1}_{N_w}^T P_W(t_0))$$

Step IV: Mathematical model of MPC

The MPC can be formulated as optimization problems which are as follows:

1) For normal mode, (33) can be rewritten as an explicit form of ΔU :

$$\min_{\Delta U} J = \|M_{MV}\Delta U + E_{MV}\|_{A_V}^2 \\ + \|M_{PL}\Delta U + E_{PL}\|_{A_L}^2 + \|M_{AP}\Delta U + E_{AP}\|_{A_P}^2 \\ \text{subject to} \\ (52a), (52b), (54a), (54b), (55) \quad (56)$$

where $A_V = \lambda_V I_{N_{MV}N_p}$, $A_L = \lambda_L I_{N_p}$, $A_P = \lambda_P I_{N_w N_p}$.

2) For corrective mode, (34) can be rewritten as an explicit form of ΔU :

$$\min_{\Delta U} J = \|M_{WT}\Delta U + E_{WT}\|_{A_W}^2 + \|M_{MV}\Delta U + E_{MV}\|_{A_{MV}}^2 \\ \text{subject to} \\ (52a), (52b), (54a), (54b), (55) \quad (57)$$

where $A_W = \lambda_W I_{N_p}$, $A_{MV} = \lambda_{MV} I_{N_p}$.

As such, the mathematical models of MPC are obtained. Obviously, they can be converted into standard QP problems and can be efficiently solved by the QP solvers.

APPENDIX B

SYSTEM PARAMETERS

The basic electrical and control system parameters are listed in Tables I~ III.

TABLE I
ELECTRICAL SYSTEM PARAMETERS

33kV Cable	$R=0.0975 \Omega/\text{km}$, $L=0.38 \text{ mH}/\text{km}$, $C=0.24 \mu\text{F}/\text{km}$
150kV Cable	$R=0.0326 \Omega/\text{km}$, $L=0.42 \text{ mH}/\text{km}$, $C=0.15 \mu\text{F}/\text{km}$
0.9/33kV Transformer	$S_n = 6.25 \text{ MVA}$, $R=0.008 \text{ p.u.}$, $X=0.06 \text{ p.u.}$
33/150kV Transformer	$S_n = 100 \text{ MVA}$, $R=0.005 \text{ p.u.}$, $X=0.12 \text{ p.u.}$
150/170kV Transformer	$S_n = 400 \text{ MVA}$, $R=0.006 \text{ p.u.}$, $X=0.14 \text{ p.u.}$
HVDC Converter	$S_n = 400 \text{ MVA}$
GSC	$S_n = 6.25 \text{ MVA}$
$R_C + jX_C$	$0.0178 + j 0.196 \text{ p.u.}$
C_f	$10 \mu\text{F}$

TABLE II
TYPICAL CONVERTER LOSS PARAMETERS [21]

System	a	b	c
GSC	0.0005	0.0097	0.0048
HVDC Converter	0.0083	0.0030	0.0032

TABLE III
CONTROL SYSTEM PARAMETERS

T_c	1 s	λ_v	0.8
T_p	5 s	λ_L	0.1
T_d	100 ms	λ_p	0.1/64

T_{inv}	5 ms	V_{W}^{th}	0.05 p.u.
ΔT_{p}	50 ms	$V_{\text{MV}}^{\text{th}}$	0.01 p.u.

REFERENCES

- [1] Wind energy scenarios for 2030, European Wind Energy Association. [Online]. Available: <https://windeurope.org/fileadmin/files/library/publications/reports/EWEA-Wind-energy-scenarios-2030.pdf>.
- [2] P. Breseti, W. L. Kling, R. L. Hendriks and R. Vailati, "HVDC connection of offshore wind farms to the transmission system," *IEEE Trans. Energy Convers.*, vol. 22, no. 1, pp. 37-43, Mar. 2007.
- [3] L. Xu, L. Fan, and Z. Miao, "DC impedance-model-based resonance analysis of a VSC-HVDC System," *IEEE Trans. Power Del.*, vol. 30, no. 3, pp. 1221-1230, Jun. 2015.
- [4] D. Zheng, A. T. Eseye, J. Zhang, and H. Li. "Short-term wind power forecasting using a double-stage hierarchical ANFIS approach for energy management in microgrids," *Protection and Control of Modern Power Systems*, vol.2, no. 1, pp. 1-10, 2017.
- [5] M. Mohseni and S. M. Islam, "Review of international grid codes for wind power integration: Diversity, technology and a case for global standard," *Renewable Sustain. Energy Rev.*, vol. 16, pp. 3876-3890, Aug. 2012.
- [6] European Commission, "COMMISSION REGULATION (EU) 2016/631 of 14 April 2016 establishing a network code on requirements for grid connection of generators," *Off. J. Eur. Union.*, pp. 10-54, 2016. [Online]. Available: <https://www.sprk.gov.lv/uploads/doc/2016631EN.pdf>
- [7] European Commission, "COMMISSION REGULATION (EU) 2016/1447 of 26 August 2016 establishing a network code on requirements for grid connection of high voltage direct current systems and direct current-connected power park modules," *Off. J. Eur. Union.*, pp. 1-65, 2016. [Online]. Available: <https://www.entsoe.eu/Documents/Network%20codes%20documents/NC%20HVDC/EC%20Regulation%20%28EU%29%202016%201447%20HVDC%20network%20code.pdf>
- [8] B. R. Karthikeya and R. J. Schutt, "Overview of wind park control strategies," *IEEE Trans. on Sustain. Energy*, vol. 5, no. 2, pp. 416-422, Apr. 2014.
- [9] X. Guan and G. M. van der Molen, Control strategy review and specification (Part 1), 2009 [Online]. Available: [http://ict-aeolus.eu/pub/ISC_300409_deliverable_D3-1_0001\(1\)_PU.pdf](http://ict-aeolus.eu/pub/ISC_300409_deliverable_D3-1_0001(1)_PU.pdf).
- [10] T. Kaneko, T. Senjyu, A. Yona, M. Datta, T. Funabashi, and C.-H. Kim, "Output power coordination control for wind farm in small power system," in *Proc. 14th Int. Conf. Intel. Syst. Appl. Power Syst. (ISAP 2007)*, Nov., pp. 51-56.
- [11] A. D. Hansen, P. E. Sørensen, F. Iov, and F. Blaabjerg, "Centralised power control of wind farm with doubly fed induction generators," *Renewable Energy*, vol. 31, no. 7, pp. 935-951, 2006.
- [12] J. Fortmann, M. Wilch, F. W. Koch, and I. Erlich, "A novel centralised wind farm controller utilising voltage control capability of wind turbines," in *Proc. PSCC Power Syst. Comput. Conf.*, 2008, pp. 914-919.
- [13] H. Zhao, Q. Wu, Q. Guo, H. Sun, S. Huang, and Y. Xue, "Coordinated voltage control of a wind farm based on model predictive control," *IEEE Trans. Sustain. Energy*, vol. 7, no. 4, pp. 1440-1451, Oct. 2016.
- [14] P. E. Sørensen, A. D. Hansen, F. Iov, F. Blaabjerg, and M. H. Donovan, "Wind farm models and control strategies," Risø Nat. Lab., Denmark, Roskilde, Tech. Rep. Risø-4-1464, Aug. 2005.
- [15] J. Martínez, P. C. Kjær, P. Rodriguez, and R. Teodorescu, "Comparison of two voltage control strategies for a wind power plant," in *Proc. IEEE/PES Power Syst. Conf. Expo. (PSCC)*, 2011, pp. 1-9.
- [16] Q. Guo, H. Sun, B. Wang, B. Zhang, W. Wu and L. Tang, "Hierarchical automatic voltage control for integration of large-scale wind power: Design and implementation," *Electr. Power Syst. Res.*, vol. 120, pp. 234-241, 2015.
- [17] A. A. van der Meer, M. Ndreko, M. Gibescu, and M. A. van der Meijden, "The effect of FRT behavior of VSC-HVDC-connected offshore wind power plants on AC/DC system dynamics," *IEEE Trans. Power Del.*, vol. 31, no. 2, pp. 878-887, Apr. 2016.
- [18] A. Moawwad, M. S. E. Moursi, W. Xiao, and J. L. Kirley, "Novel configuration and transient management control strategy for VSC-HVDC," *IEEE Trans. Power Syst.*, vol. 29, no. 5, pp. 2478-2488, Sep. 2014.
- [19] L. Xu, L. Yao, and C. Sasse, "Grid integration of large DFIG-based wind farms using VSC transmission," *IEEE Trans. Power Syst.*, vol. 22, no. 3, pp. 976-984, Aug. 2007.
- [20] J. N. Sakamuri, Z. H. Rather, J. Rime, M. Altin, O. Goksu, and N. A. Cutululis, "Coordinated voltage control in offshore HVDC connected cluster of wind power plants," *IEEE Trans. Sustain. Energy*, vol. 7, no. 4, pp. 1592-1601, Oct. 2016.
- [21] K. Schönleber, C. Collados, R. T. Pinto, S. Ratés-Palau, and O. Gomis-Bellmunt, "Optimization-based reactive power control in HVDC-connected wind power plants," *Renewable Energy*, vol. 109, pp. 500-509, 2017.
- [22] K. Schönleber, S. Ratés-Palau, M. De-Prada-Gil, and O. Gomis-Bellmunt, "Reactive power optimization in HVDC-connected wind power plants considering wake effects," *14th Wind Integr. Work. Energynautics GmbH, Brussels*, 2015.
- [23] B. Zhang, P. Hou, W. Hu, M. Soltani, C. Chen, and Z. Chen, "A Reactive Power Dispatch Strategy With Loss Minimization for a DFIG-Based Wind Farm," *IEEE Trans. on Sustain. Energy*, vol. 7, no. 3, pp. 914-923, Jul. 2017.
- [24] S. M. Mueyeen, R. Takahashi, and J. Tamura, "Operation and control of HVDC-connected offshore wind farm," *IEEE Trans. Sustain. Energy*, vol. 1, no. 1, pp. 30-37, Apr. 2010.
- [25] A. J. Sguarezi Filho, M. E. de Oliveira Filho, and E. Ruppert Filho, "A predictive power control for wind energy," *IEEE Trans. Sustain. Energy*, vol. 2, no. 1, pp. 97-105, Jan. 2011.
- [26] V. Yaramasu, B. Wu, M. Rivera, and J. Rodriguez, "A new power conversion system for megawatt PMSG wind turbines using four-level converters and a simple control scheme based on two-step model predictive strategy—Part I: Modeling and theoretical analysis," *IEEE J. Emerging Sel. Topics Power Electron.*, vol. 2, no. 1, pp. 3-13, Mar. 2014.
- [27] X. Liu and X. Kong, "Nonlinear model predictive control for DFIG based wind power generation," *IEEE Trans. Automat. Sci. Eng.*, vol. 11, no. 4, pp. 1046-1055, Oct. 2014.
- [28] J. Hu, J. Zhu, and D. Dorrel, "Predictive direct power control of doubly fed induction generators under unbalanced grid voltage conditions for power quality improvement," *IEEE Trans. Sustain. Energy*, vol. 6, no. 6, pp. 687-695, Aug. 2014.
- [29] H. Zhao, Q. Wu, Q. Guo, H. Sun, and Y. Xue, "Distributed model predictive control of a wind farm for optimal active power control—Part I: Clustering-based wind turbine model linearization," *IEEE Trans. Sustain. Energy*, vol. 6, no. 3, pp. 1-10, Jul. 2015.
- [30] H. Zhao, Q. Wu, Q. Guo, H. Sun, and Y. Xue, "Distributed model predictive control of a wind farm for optimal active power control—Part II: Implementation with clustering-based piece-wise affine wind turbine model," *IEEE Trans. Sustain. Energy*, vol. 6, no. 3, pp. 1-10, Jul. 2015.
- [31] H. Zhao, Q. Wu, J. Wang, Z. Liu, S. Mohammad, Y. Xue, "Combined active power and reactive power control of wind farms based on model predictive control," *IEEE Trans. Energy Convers.*, to be published.
- [32] E. Camponogara, D. Jia, B. H. Krogh, and S. Talukdar, "Distributed model predictive control," *IEEE Control Syst. Mag.*, vol. 9, no. 1, pp. 44-52, Jan. 2002.
- [33] K. Christakou, J. LeBoudec, M. Paolone, and D.-C. Tomozei, "Efficient computation of sensitivity coefficients of node voltages and line currents in unbalanced radial electrical distribution networks," *IEEE Trans. Smart Grid*, vol. 4, no. 2, pp. 741-750, Jun. 2013.
- [34] E. V. Larsen and A. S. Achilles, "System and method for voltage control of wind generators," US Patent App. 14/018482, Sep. 5 2013.
- [35] S. Cole, J. Beerten, and R. Belmans, "Generalized dynamic VSC MTDC model for power system stability studies," *IEEE Trans. Power Syst.*, vol. 25, no. 3, pp. 1655-1662, Aug. 2010.
- [36] P. Lagonotte, J. C. Leost, and J. P. Paul, "Structural analysis of the electrical system: Application to secondary voltage control in France," *IEEE Trans. Power Syst.*, vol. 4, no. 2, pp. 479-486, May. 1989.
- [37] H. J. Ferreau, "Model predictive control algorithms for applications with millisecond timescales," Ph.D. thesis, Dept. of Electr. Eng., KU Leuven, Leuven, Belgium, 2011.
- [38] J. D. Grunnet, M. Soltani, T. Knudsen, M. Kragelund, and T. Bak, "Aeolus toolbox for dynamic wind farm model, simulation and control," in *Proc. Eur. Wind Energy Conf.*, 2010, pp. 1-6.